

Identification of photons in double beta-decay experiments using segmented germanium detectors - studies with a GERDA Phase II prototype detector

I. Abt, A. Caldwell, K. Kröniger^{*}, J. Liu, X. Liu,
B. Majorovits

Max-Planck-Institut für Physik, München, Germany

Abstract

The sensitivity of experiments searching for neutrinoless double beta-decay of germanium was so far limited by the background induced by external γ -radiation. Segmented germanium detectors can be used to identify photons and thus reduce this background component.

The GERmanium Detector Array, GERDA, will use highly segmented germanium detectors in its second phase. The identification of photonic events is investigated using a prototype detector. The results are compared with Monte Carlo data.

Key words: double beta-decay, germanium detectors, segmentation

PACS: 23.40.-s, 14.60Pq, 29.40.-n

1 Introduction

Neutrinoless double beta-decay ($0\nu\beta\beta$) is expected to occur, if the neutrino is a massive Majorana particle. The observation of the $0\nu\beta\beta$ -process would not only reveal the nature of the neutrino as a Majorana particle but could also provide information about the absolute neutrino mass scale (see, e.g. [1]).

The germanium isotope ^{76}Ge is a prominent candidate for the observation of the $0\nu\beta\beta$ -process. Experiments searching for neutrinoless double beta-decay

^{*} Max-Planck-Institut für Physik, München, Germany, Tel. +49-(0)89-32354-337
Email address: kroening@mppmu.mpg.de (K. Kröniger).

of ^{76}Ge use high purity germanium detectors as source and detector simultaneously. Their sensitivity is limited by unidentified background events which in previous experiments were mostly induced by external γ -radiation. The Heidelberg-Moscow and IGEX experiments set 90% C.L. lower limits on the half-life of the process of $T_{1/2} > 1.9 \cdot 10^{25}$ years [2] and $T_{1/2} > 1.6 \cdot 10^{25}$ years [3], respectively. An evidence for the observation of the $0\nu\beta\beta$ -process was claimed by parts of the Heidelberg-Moscow collaboration with $T_{1/2} = 1.2 \cdot 10^{25}$ years [4].

The GERmanium Detector Array, GERDA [5], is a new germanium double beta-decay experiment being installed in Hall A of the INFN Gran Sasso National Laboratory (LNGS), Italy. Its main design feature is to operate germanium detectors directly in liquid argon which serves as cooling medium and as a shield against external γ -radiation. A detailed description of the experiment can be found in [5,6].

The detectors for the second phase of the experiment (Phase II) will be enriched in ^{76}Ge to a level of about 86% and will have a mass of approximately 2 kg each. For the first time, highly segmented germanium detectors will be used in a double beta-decay experiment. The segmentation scheme is chosen to minimize the background level in the energy region around $Q_{\beta\beta} = 2039$ keV. The current detector design foresees a 6-fold segmentation in the azimuthal angle ϕ and a 3-fold segmentation in the height z . All segments and the core are read out separately to allow a better identification of photons. The estimated gain in background reduction for the GERDA experiment is discussed in [6].

In this paper the results of a study with a GERDA Phase II prototype detector are presented. The identification of events with photons in the final state is investigated. Section 2 summarizes the photon identification using coincidences between segments. The underlying physics processes and their signatures are described as are the event selection and the analysis strategy. Section 3 describes the experimental setup of the prototype detector and the data sets collected. The Monte Carlo simulation is introduced in section 4. The results of the study and comparisons with Monte Carlo data are given in section 5. Section 6 concludes and discusses the significance for the GERDA experiment.

2 Identification of photon events using segment coincidences

The volume over which energy in a single event is deposited inside a detector depends on the incident particles. Segmented detectors can be used to identify events with photons in the final state by requiring coincidences between the segments of a detector. This technique is well established in nuclear experiments such as AGATA [7] and GRETA [8], and provides a basis for γ -ray tracking [9].

The potential of segmented detectors for double beta-decay experiments has also been investigated by the MAJORANA collaboration [10] using a clover detector, consisting of four detectors with two longitudinal segments each, and Monte Carlo simulations [11].

2.1 Signatures and physics processes

The signatures of events encountered in double beta-decay experiments can be classified according to the particles in the final state. A detailed classification for these events is given in [6]. For the identification of photon events only two such classes are considered here:

- Class L: Local energy deposit. Three different types of events are part of this class: (a) Events with only electrons in the final state. Electrons in the MeV-energy region have a range of the order of a millimeter in germanium [6,12]. Energy is therefore deposited locally. Double beta-decay events which have two electrons in the final state are of this type (these events correspond to Class I events in reference [6]). (b) Events with photons in the final state in which a photon Compton-scatters only once inside the fiducial volume of the detector. Energy is thus deposited locally. (c) 'Double escape' events: If a photon produces an electron-positron pair and both photons from the subsequent annihilation escape, energy is deposited locally.
- Class M: Multiple energy deposits. Photons emitted in radioactive decays have energies in the MeV-energy region and interact dominantly through Compton scattering in germanium. The range of these photons is of the order of centimeters. The different interactions are separated by distances large compared to the scale of Class L events. This class is composed of Classes II-IV in reference [6].

It should be noted that with the technique presented in this paper the three event types in Class L cannot be separated but only be distinguished from Class M events.

2.2 *Event selection and identification of photon events*

Due to the well separated multiple energy deposits Class M events are expected to deposit energy predominantly in more than one segment. Class L events will predominantly deposit energy in only one segment. Events in which more than one segment measures deposited energy can thus be identified as Class M events.

3 **Experimental setup and data sets**

3.1 *Experimental setup*

The GERDA Phase II prototype detector under study is a high purity n -type germanium crystal with a true coaxial geometry. It is 70 mm high and has an outer diameter of 75 mm. The inner diameter is 10 mm. The detector is 6-fold segmented in the azimuthal angle ϕ and 3-fold segmented in the height z . It is placed inside a two-walled aluminum cryostat with a combined thickness of 6 mm. The operation voltage of the detector is (+)3 000 V.

A schematic diagram of the detector and the experimental setup is given in Figure 1. The core and each segment are read out using charge sensitive PSC 823 pre-amplifiers. The pre-amplified signals are digitized using a data acquisition system based on 5 14-bit ADC PIXIE-4 modules at a sampling rate of 75 MHz. In this configuration the energy resolution of the core is approximately 2.6 keV (FWHM at 1 333 keV), the energy resolution of the segments varies between 2.4 keV and 4.7 keV with an average segment energy resolution of 3.3 keV. The threshold of the core and the segments was set to 20 keV. Cross-talk between the core and the segment pre-amplifiers and a constraint in the DAQ system, which resulted in the inability to handle late arriving signals, caused a fraction of less than 10% of individual segment signals to not be recorded.

A detailed description of the setup and the prototype properties will be published [13].

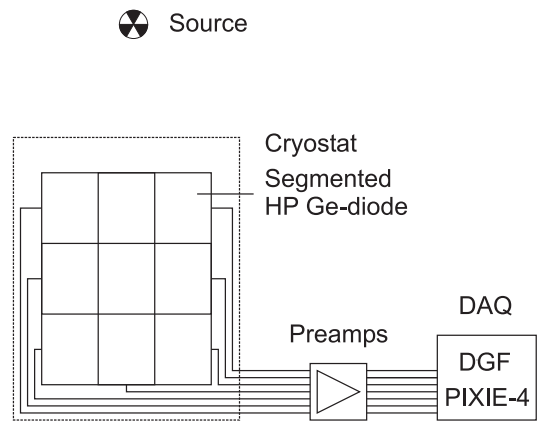


Fig. 1. Schematic diagram of the detector and the experimental setup.

3.2 Measurements and data sets

Several measurements were performed with different radioactive sources positioned 10 cm above the center of the detector. Energy and time information in all segments and the core were recorded on an event-by-event basis. An event was recorded, if the energy measured in the core exceeded the threshold. Measurements were performed with three different sources: (1) a 60 kBq ^{60}Co source, (2) a 100 kBq ^{228}Th source and (3) a 75 kBq ^{152}Eu source. The corresponding data sets are referred to as “source data sets” in the following and contain approximately $4 \cdot 10^6$ events each. An additional measurement without any source was performed in order to estimate the background in the laboratory. This “background data set” contains approximately 10^6 events.

Figure 2 shows the raw energy spectra obtained with the core electrode for the three source data sets and the background data set.

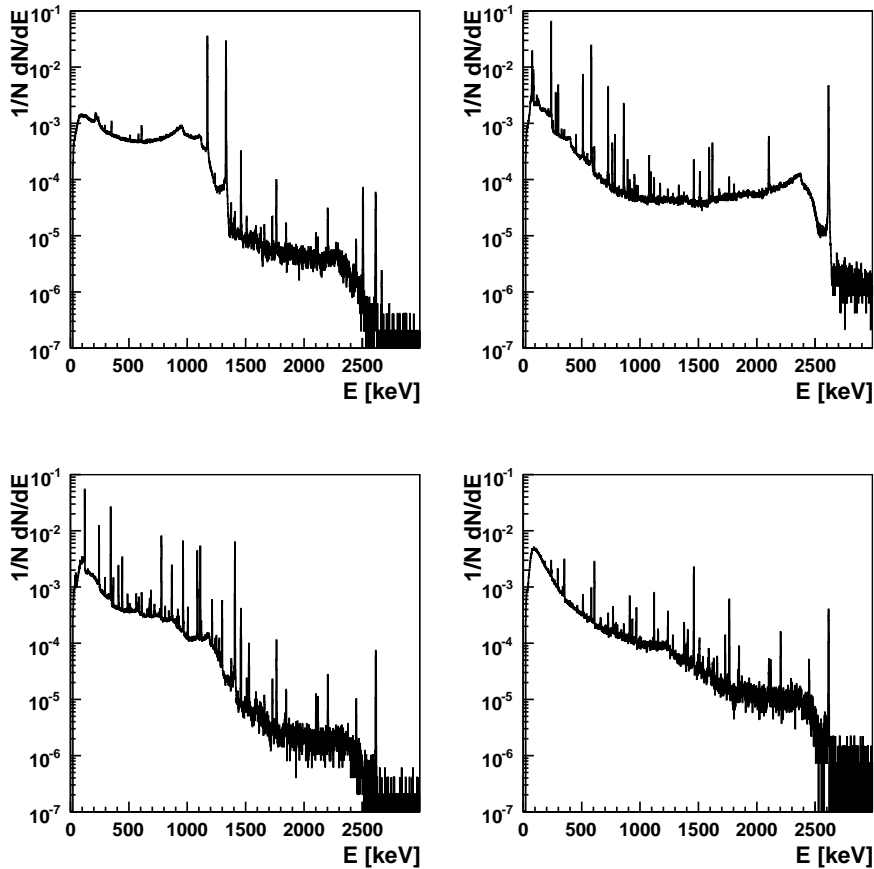


Fig. 2. Raw energy spectra obtained with the core electrode for the ^{60}Co (top, left), ^{228}Th (top, right) and the ^{152}Eu (bottom, left) source data sets. The sources were placed 10 cm above the detector. The energy spectrum for the background data set is also shown (bottom, right). The binning is 1 keV and the spectra are normalized to the area.

4 Monte Carlo simulation

A Monte Carlo simulation of the prototype setup was performed using the GEANT4 [14] based MAGE framework [15]. The energy deposited in each segment is recorded and the core energy is calculated by adding all segment energies.

The drift anisotropy of charge carriers inside the germanium diode [16] can cause electrons and holes to deviate from their drift path. It is therefore possible to measure energy in one segment even if the energy was deposited in the neighboring segment. Hence, a correction is applied to the segment energies. An effective model is used which assigns a segment to each energy deposit depending on its position with respect to the axes of the crystal and the segment borders. The maximum angular shift is 3.5° . The directions of the crystal axes were measured and used as input for the Monte Carlo. This includes an overall variation of this effect by 40% with respect to the two hemispheres.

Each segment is assigned a relative efficiency with respect to the core on the order of 90%. This effectively models the DAQ-inefficiency. The segment and core energies are individually smeared according to the energy resolution of the prototype detector measured in each channel.

5 Results

The results of the measurements are presented in the following and compared to Monte Carlo data. In order to account for background from radioactive isotopes in the laboratory the fraction of background events in each data set is estimated.

5.1 Background estimate

The number of background events in a given source data set is estimated using characteristic photon lines in the spectrum. These lines are associated with the decays of ^{214}Pb (352 keV), ^{214}Bi (609 keV, 1 120 keV, 1 765 keV, 2 204 keV) and ^{40}K (1 461 keV). The photon lines are fitted with a Gaussian plus linear function and the number of events, n_i , under each peak is calculated.

For the background data set, the fraction of events under the i th peak is denoted $f_i = N_i/N$, where N_i is the number of events under the i th peak and N is the total number of events in the spectrum. For each source data set the total number of background events, n_{bkg} , is estimated by minimizing a χ^2 -function defined as

$$\chi^2 = \chi^2(n_{\text{bkg}}) = \sum_i \frac{(n_{\text{bkg}} \cdot f_i - n_i)^2}{\sigma_i^2 + n_i}, \quad (1)$$

where σ_i is the Poissonian uncertainty on the expression $n_{\text{bkg}} \cdot f_i$.

The fraction of background events in the source data sets are estimated as 14.0% ($\chi^2/d.o.f. = 1.0$) for ^{60}Co , 8.3% ($\chi^2/d.o.f. = 0.7$) for ^{228}Th and 15.8% ($\chi^2/d.o.f. = 8.4$) for ^{152}Eu . An uncertainty on the background fraction of 0.1% is estimated.

5.2 Photon identification and reduction

The segment multiplicity, N_S , is defined as the number of segments with measured energies larger than the threshold of 20 keV.

A measure for the identification of photonic events is the *number* suppression factor, SF_N , defined as the ratio of the number of events within a 10 keV region around a certain energy and the number of events which, in addition, have a segment multiplicity of $N_S = 1$. In order to quantify the identification of photons which deposit their full energy within the detector the *line* suppression factor, SF_L , is defined similarly to SF_N , but the number of events is replaced by the number of events under the photon peak under study.

For the calculation of the suppression factors the number of events in the source data sets are corrected for the background by subtracting the background contribution.

The number suppression factor is calculated for the $Q_{\beta\beta}$ region of ^{76}Ge (2 039 keV) whereas the line suppression factors are calculated for the photon lines of ^{60}Co (1 173 keV, 1 333 keV and the summation peak at 2 506 keV), ^{208}Tl (511 keV, 583 keV, 861 keV, 2 615 keV and the corresponding single and double escape peaks at 2 104 keV and 1 593 keV), ^{212}Bi (1 620 keV) and ^{152}Eu (122 keV, 245 keV, 344 keV, 779 keV, 964 keV, 1 086 keV, 1 112 keV and 1 408 keV).

The results are displayed in Table 1 for data and Monte Carlo data. For a discussion of the agreement between data and Monte Carlo see section 5.5.

Table 1

Suppression factors for different sources and energies calculated for data and Monte Carlo. The background has been subtracted from the data. For a discussion on the agreement between data and Monte Carlo see section 5.5. The uncertainties are statistical uncertainties only.

Source	Energy [keV]	SF_N (data)	SF_L (data)	SF_N (MC)	SF_L (MC)
^{60}Co	1 173	-	2.56 ± 0.01	-	2.56 ± 0.01
	1 333	-	2.63 ± 0.01	-	2.63 ± 0.01
	2 506	-	34.6 ± 5.7	-	43.0 ± 11.0
	2 039	14.2 ± 2.1	-	12.5 ± 2.1	-
^{228}Th	511	-	1.92 ± 0.01	-	1.91 ± 0.02
	583	-	2.04 ± 0.01	-	2.01 ± 0.01
	861	-	2.35 ± 0.03	-	2.37 ± 0.05
	1 593	-	1.09 ± 0.02	-	1.09 ± 0.04
	1 620	-	2.85 ± 0.01	-	2.84 ± 0.13
	2 104	-	3.13 ± 0.01	-	3.20 ± 0.11
	2 615	-	3.04 ± 0.02	-	3.23 ± 0.04
	2 039	1.68 ± 0.02	-	1.66 ± 0.05	-
^{152}Eu	122	-	1.01 ± 0.002	-	1.01 ± 0.003
	245	-	1.26 ± 0.01	-	1.22 ± 0.01
	344	-	1.54 ± 0.01	-	1.55 ± 0.01
	779	-	2.29 ± 0.01	-	2.26 ± 0.02
	964	-	2.46 ± 0.02	-	2.41 ± 0.02
	1 086	-	2.54 ± 0.02	-	2.50 ± 0.03
	1 112	-	2.52 ± 0.02	-	2.54 ± 0.04
	1 408	-	2.64 ± 0.02	-	2.72 ± 0.02

The line suppression factors increases from 1.01 ± 0.002 at 122 keV to 3.04 ± 0.01 at 2 615 keV, where the suppression increases with increasing energy. This is expected as the average number of Compton-scattering processes increases. Figure 3 shows the line suppression factors as a function of the core energy for data and Monte Carlo data.

The double escape peak of the 2615 keV photon from the de-excitation of ^{208}Tl at 1593 keV is basically not suppressed. These Class L events have a very localized energy deposition. In comparison, the 1620 keV line from the ^{212}Bi is suppressed by a factor of 2.85 ± 0.01 . These events are predominantly encompassed in Class M. Figure 4 shows the energy spectrum for the ^{228}Th source with and without a segment multiplicity requirement of $N_S = 1$. The left figure shows the energy region up to 3 MeV, the right figure shows a close-up of the region around 1.6 MeV. Note that background has not been subtracted from the data spectra.

The number suppression factor for the ^{60}Co source is $SF_N = 14.2 \pm 2.1$. It is large compared to the suppression factor for the ^{208}Th source of $SF_N = 1.68 \pm 0.002$. For the latter, the $Q_{\beta\beta}$ region lies within the Compton continuum of the ^{208}Tl photon. A single scattering process can cause a local energy deposit. In contrast, for the ^{60}Co source an energy deposit in this energy region is only possible if both photons (1173 keV and 1333 keV) deposit energy in the same segment. In contrast, the number suppression factor for $0\nu\beta\beta$ -decay events is expected to be close to unity as the electrons in the final state mostly deposit energy in only one segment.

Figure 5 shows the energy spectrum for the ^{60}Co source with and without a segment multiplicity requirement of $N_S = 1$. The left figure shows the energy region up to 3 MeV, the right figure shows a close-up of the region around the $Q_{\beta\beta}$ -value of ^{76}Ge . Note that background has not been subtracted from the spectra.

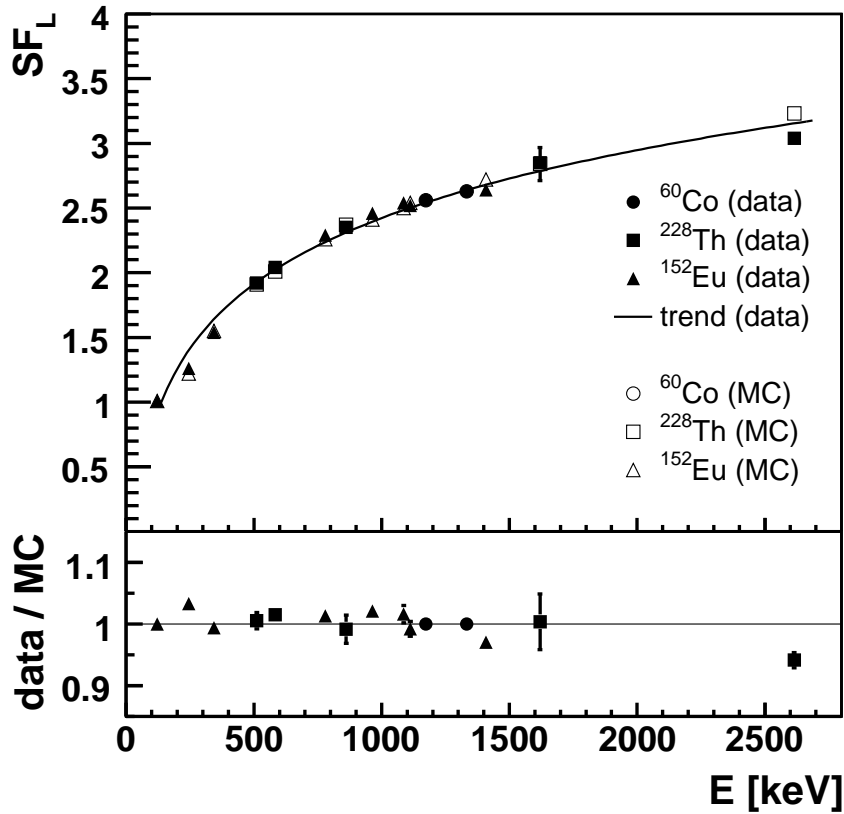


Fig. 3. Top: Line suppression factor as a function of the core energy for data (solid marker) and Monte Carlo data (open marker). The trend curve guides the eye. Bottom: Data to Monte Carlo ratio. The average deviation is less than 5%. For a discussion on the agreement between data and Monte Carlo see section 5.5.

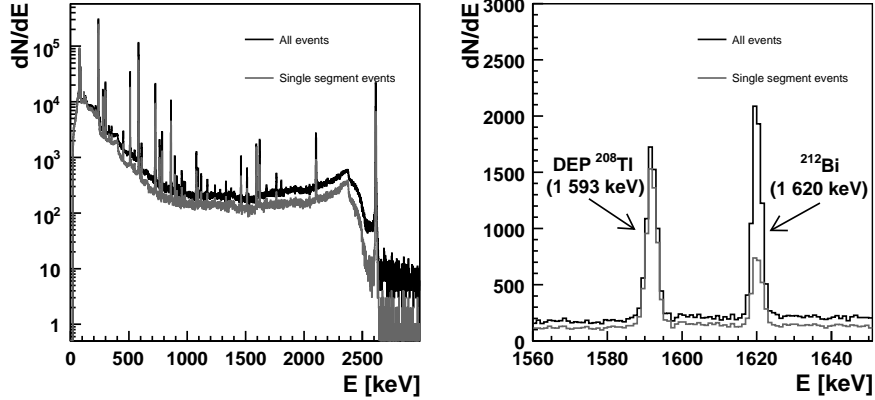


Fig. 4. Core energy spectrum for the ^{208}Th source data set for all events (black spectrum) and those with a segment multiplicity of $N_S = 1$ (grey spectrum). The left spectrum shows the energy region up to 3 MeV, the right spectrum is a close-up of the region around 1.6 MeV. The double escape peak from ^{208}Tl (1 593 keV) is hardly suppressed ($SF_L = 1.09 \pm 0.02$) while the ^{212}Bi line (1 620 keV) is suppressed by a factor of $SF_L = 2.85 \pm 0.01$. Note that background has not been subtracted from the spectra.

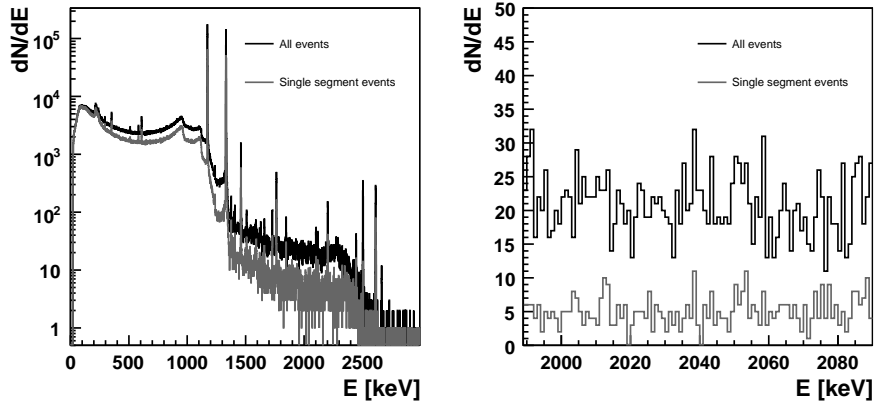


Fig. 5. Core energy spectrum for the ^{60}Co source data set for all events (black spectrum) and those with a segment multiplicity of $N_S = 1$ (grey spectrum). The left spectrum shows the energy region up to 3 MeV, the right spectrum is a close-up of the $Q_{\beta\beta}$ -region (2 039 keV). In this energy region, the single-segment spectrum is suppressed by a factor of $SF_N = 14.2 \pm 2.1$. Note that background has not been subtracted from the spectra.

5.3 Segmentation study

In order to study the identification of photons for different segmentation schemes the segment energies are added in three patterns: sector, ring and hemisphere. A sector is obtained by adding the energies of equal ϕ segments. A ring is obtained by adding the energies of equal z segments. Two hemispheres are obtained by adding the energies of sectors 0, 1, 2 and sectors 3, 4, 5, respectively. The effective number of segments for the segmentation schemes are 6, 3 and 2, respectively.

The suppression factors for each segmentation scheme are obtained as described in section 5.2 with segments replaced by sectors, rings or hemispheres. Table 2 shows the number suppression factor and line suppression factors for selected photon lines for all four schemes (including the 18-fold segmentation scheme) obtained from the measurements. As expected, the number and line suppression factors increase with an increasing effective number of segments.

Table 2

Number and line suppression factors for selected photon lines for all four segmentation schemes. An estimated background fraction has been subtracted from the data. The numbers in brackets are the effective number of segments for the specific scheme. The uncertainties are statistical uncertainties only.

Source	Energy [keV]	SF (18)	SF (6)	SF (3)	SF (2)
^{152}Eu	344	1.54 ± 0.01	1.36 ± 0.004	1.24 ± 0.003	1.12 ± 0.003
^{60}Co	1333	2.63 ± 0.01	1.94 ± 0.01	1.71 ± 0.004	1.30 ± 0.003
^{228}Th	2615	3.04 ± 0.02	2.16 ± 0.01	1.86 ± 0.01	1.38 ± 0.01
^{60}Co	2039	14.2 ± 2.1	9.63 ± 1.21	3.92 ± 0.33	2.61 ± 0.19
^{228}Th	2039	1.68 ± 0.02	1.43 ± 0.02	1.40 ± 0.02	1.18 ± 0.02

Figure 6 shows the line suppression factors for the selected photon lines as a function of the effective number of segments for data and Monte Carlo.

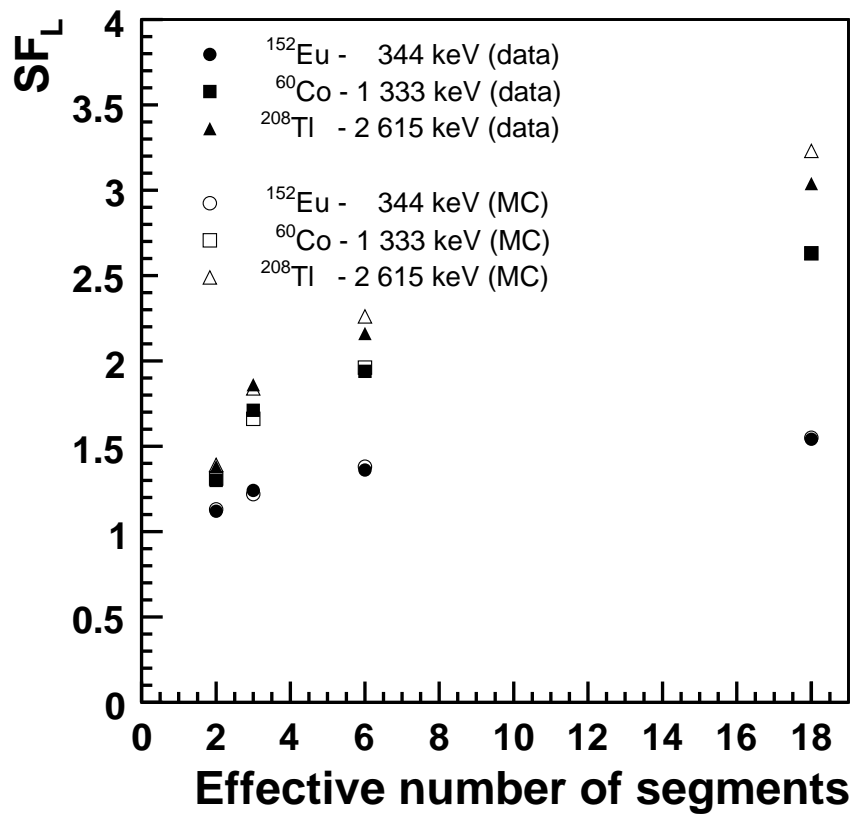


Fig. 6. Line suppression factors for selected photon lines as a function of the effective number of segments for data (solid marker) and Monte Carlo data (open marker).

5.4 Further studies

The effect of the energy threshold on the line suppression factors was studied by varying the threshold of the core and segment channels from 15 keV to 100 keV. A sharp rise of the line suppression factors is observed towards 15 keV due to an increased noise level. This behavior is not observed in Monte Carlo. Between 20 keV and 100 keV the line suppression factors decrease by up to 7%. In particular, the double escape peak at 1 593 keV decreases by 4%.

A variation of the position of the source was performed. The distance between the source and the crystal was varied. In addition, the sources were placed at half the crystal height. The radial distance between the source and the crystal was varied. No significant difference in the suppression factors was found.

The uncertainty on the background fraction in the data samples is estimated to be 0.1%. A variation of the estimated background fraction by this amount did not reveal significant differences in the line suppression factors. For ^{60}Co the number suppression factor decreases with an increasing background fraction because background events in the energy region around 2 MeV are mostly singly Compton-scattered photon events from ^{208}Tl .

5.5 Data to Monte Carlo comparison

In the following, the results of the Monte Carlo simulation introduced in section 4 are compared with data for the ^{60}Co measurement. Equivalent results are obtained for all three sources used.

Figure 7 (top, left) shows the core energy spectrum for the ^{60}Co source. The data is indicated by the black marker. Also shown is the statistical uncertainty. The background data is represented by the hatched histogram, the Monte Carlo data by the open histogram. The background contribution is estimated as previously described. For energies below 100 keV the Monte Carlo plus background data exceeds the data due to the trigger turn-on which is not described by Monte Carlo. The Compton continuum of the two ^{60}Co lines is described by Monte Carlo with an average deviation of about 5%. The number of events under the peak for the two ^{60}Co lines are lower in data by 10%. Tails left and right of the gamma peaks in data are due to pile-up and not described by the simulation. The region above 1.3 MeV is dominated by background events. In this region the average deviation between data and Monte Carlo plus background data is of the order of 10% or less. In particular, the

number of events under the peak for the ^{60}Co summation line and the ^{208}Tl line agree within the statistical uncertainties.

Figure 7 (top, right) shows the occupancy of each segment, i.e. the fraction of events in which energy is deposited in the segment under study. No cut on the energy has been applied. Clearly visible are three groups of segments (1-6, 7-12, 13-18) which correspond to the three z-positions bottom, middle and top, respectively. As expected, the bottom segments have the lowest, the top segments the highest occupancy. A pattern within each group is present which can be explained by the drift anisotropy of the charge carriers. The structure is reproduced by Monte Carlo using an effective model for the anisotropy. Without taking the anisotropy into account no structure is visible. The deviation between data and Monte Carlo plus background data ranges up to 5-10%.

Figure 7 (middle, left) shows the segment multiplicity N_S . Data and Monte Carlo range up to multiplicities of 7-8 with an average multiplicity of 1.4. For multiplicities up to 3 the deviation between data and Monte Carlo plus background data ranges up to 5%. For higher multiplicities the data exceeds the Monte Carlo with increasing multiplicity.

Figure 7 (middle, right) shows the average segment multiplicity as a function of the energy measured with the core electrode up to 3 MeV. For energies up to 1 MeV the average multiplicity increases with energy from 1 to about 1.5. For energies between 1 MeV and 1.3 MeV the multiplicity increases up to 2.2. The deviation between data and Monte Carlo plus background data for energies below 1.3 MeV ranges up to 10%. For higher energies the average deviation is of the order of 15%, where the Monte Carlo plus background data shows a larger average multiplicity.

Figure 7 (bottom, left) shows the energy spectrum measured with (arbitrarily chosen) segment 10 up to energies of 3 MeV. The features described for the core electrode are also seen here. The deviation between data and Monte Carlo plus background data ranges up to 10%.

Figure 7 (bottom, right) shows the occupancy for segment 10 as a function of the energy measured with the core electrode up to 3 MeV. The occupancy ranges from 5% to 8% for energies below 1.3 MeV. For larger energies the occupancy ranges up to 15%. The deviation between data and Monte Carlo plus background data ranges up to 10%.

The suppression factors derived from the data are compared with those yielded from the Monte Carlo simulation in Table 1. The average deviation between data and Monte Carlo data is less than 5%. The absolute values depend on the DAQ-inefficiency.

The overall agreement between data and Monte Carlo plus background data is good. The remaining discrepancy between data and Monte Carlo plus background data could stem from (1) the modeling of the exact detector geometry including dead layers and segment borders, (2) the missing modeling of the drift of charge carriers, especially close to the surface of the crystal, (3) the missing simulation of the pre-amplifier response, (4) effects which are not accounted for in the simulation such as pile-up and trigger turn-on in the DAQ system and (5) the missing angular correlation between the photons of the cascades¹.

¹ Preliminary studies show that the angular correlation between the photons emitted in the decay of ^{60}Co has no significant effect on the suppression factors.

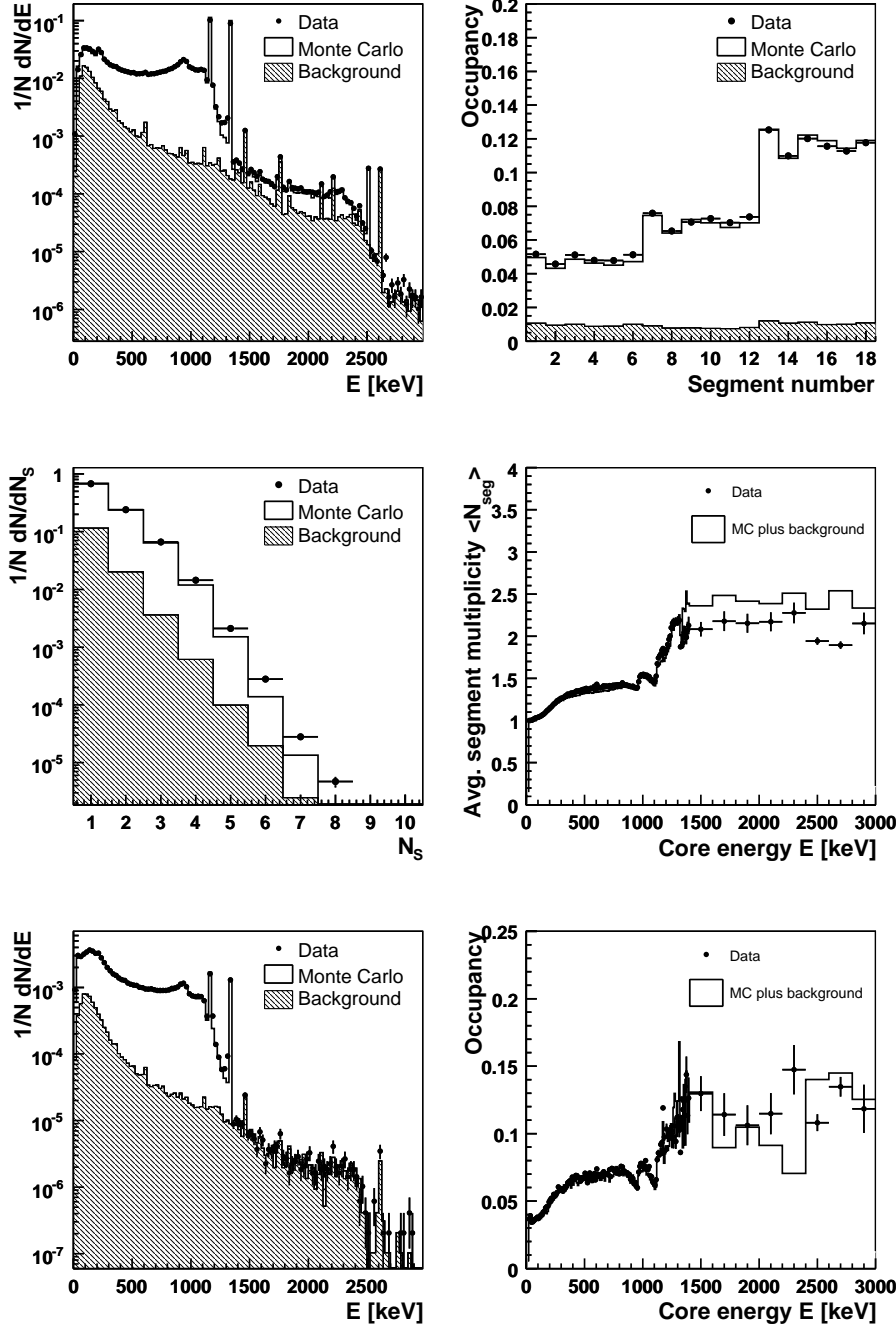


Fig. 7. Comparison between data and Monte Carlo plus background data for several quantities under study for the ^{60}Co source data set. The data is indicated by the black marker. The background data is represented by the hatched histogram, the Monte Carlo data by the open histogram. The background contribution is estimated as previously described. Top, left: core energy spectrum. Top, right: occupancy of all segments. Middle, left: segment multiplicity. Middle, right: average multiplicity as a function of the core energy. Bottom, left: energy spectrum taken with segment 10. Bottom, right: occupancy of segment 10 as a function of core energy. See text for further details.

6 Conclusions and outlook

A study with a segmented GERDA prototype detector was performed. It was shown that the identification of events with multiply scattered photons in the final state using segmented detectors is feasible. The reduction of events in which only the full photon energy is deposited inside the detector is energy dependent and increases from 1.01 ± 0.002 at 122 keV to 3.13 ± 0.01 at 2615 keV in the experimental setup described. The suppression of Compton-scattered events in the $Q_{\beta\beta}$ -region of ^{76}Ge (2039 keV) coming from ^{60}Co and ^{228}Th sources was measured to be 14.2 ± 2.1 and 1.68 ± 0.02 , respectively.

An additional study showed that the identification of photon events is improved by increasing the number of segments and that it is stable with respect to energy threshold variations and the background estimate.

In comparison to the suppression factors calculated in [6] the suppression for a single crystal is lower than for an array of detectors due to the geometrical acceptance.

A data to Monte Carlo comparison, considering background from radioactive isotopes in the laboratory, showed an agreement with deviations on the level of 5-10%. This shows that simulations based on the MAGE tool are suitable and can reliably predict background reductions as presented in [6].

The identification of photonic events can be further improved by the analysis of the time structure of the detector responses. This is currently under study.

7 Acknowledgements

The authors would like to thank the GERDA and MAJORANA Monte Carlo groups for their fruitful collaboration and cooperation on the MAGE project.

References

- [1] S. M. Bilenky, C. Giunti, W. Grimus, B. Kayser and S. T. Petcov, Phys. Lett. B **465** (1999) 193
- [2] M. Gunther *et al.*, Phys. Rev. D **55** (1997) 54.

- [3] D. Gonzalez *et al.*, Nucl. Instrum. Meth. A **515** (2003) 634
- [4] H. V. Klapdor-Kleingrothaus, A. Dietz, H. L. Harney and I. V. Krivosheina, Mod. Phys. Lett. A **16** (2001) 2409
- [5] S. Schönert *et al.* [GERDA Collaboration], Nucl. Phys. Proc. Suppl. **145** (2005) 242.
- [6] I. Abt *et al.* [GERDA Collaboration], Nucl. Instr. and Meth. A **570/3** (2007) 479.
- [7] J. Simpson, J. Phys. G **31** (2005) S1801.
- [8] K. Vetter *et al.*, Nucl. Instrum. Meth. A **452** (2000) 105.
- [9] N. J. Hammond, T. Duguet and C. J. Lister, Nucl. Instrum. Meth. A **547** (2005) 535
- [10] R. Gaitskell *et al.* [Majorana Collaboration], arXiv:nucl-ex/0311013.
- [11] C. E. Aalseth *et al.* [Majorana Collaboration], Nucl. Phys. Proc. Suppl. **138** (2005) 217.
- [12] R. B. Firestone, “Table of Isotopes”, 8th edition, 1999, John Wiley & Sons, Inc., ISBN 0-471-14918-7.
- [13] I. Abt *et al.* [GERDA Collaboration], arxiv:nucl-ex/0701004.
- [14] S. Agostinelli *et al.* [GEANT4 Collaboration], Nucl. Instrum. Meth. A **506**, 250 (2003).
- [15] M. Bauer *et al.*, Journal of Physics, Conf. Series. **39** (2006) 362.
- [16] H. G. Reik and H. Risken, Phys. Rev. **126** (1962) 1737-1746